ARTICLE

Low-Temperature Copper Bonding Strategy with Graphene Interlayer

Haozhe Wang,[†,#] Wei Sun Leong,[†,#] Fengtian Hu,[‡,#] Longlong Ju,[‡,#] Cong Su,[§,#] Yukun Guo,[‡] Ju Li,[§] Ming Li,[‡] Anmin Hu,*[‡] and Jing Kong*[†]
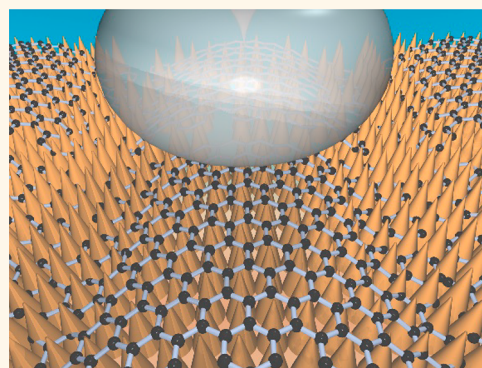
†Department of Electrical Engineering and Computer Science, Massachusetts Institute of Technology, Cambridge, Massachusetts 02139, United States

‡School of Materials Science and Engineering, Shanghai Jiao Tong University, Shanghai, 200240, China

§Department of Nuclear Science and Engineering, Massachusetts Institute of Technology, Cambridge, Massachusetts 02139, United States

S *Supporting Information*

ABSTRACT: The reliability of lead-free Cu bonding technology is often limited by high bonding temperature and perpetual growth of intermetallic compounds between Sn solder and Cu substrate. Here, we report a low-bonding-temperature and highly reliable Cu bonding strategy with the use of graphene as an interlayer. By integrating a nanoscale graphene/Cu composite on the Cu substrate prior to thermocompression bonding, we observe a macroscale phenomenon where reliable Sn−Cu joints can be fabricated at a bonding temperature as low as 150 °C. During the bonding process, nanoscale features are replicated in the Sn solder by the Cu nanocone array morphology. Compared to microscale Sn, nanoscale Sn is mechanically weaker and thus can distribute on the Cu substrate at a much lower temperature. Furthermore, insertion of a graphene interlayer, which is one atom thick, can successfully retard the intermetallic compounds' growth and preserve a high bonding yield, following 96 h of aging, as confirmed through SEM and shear strength analyses. Our graphene-based Cu bonding strategy demonstrated in this work is highly reliable, cost-effective, and environmentally friendly, representing a much closer step toward industrial applications.

KEYWORDS: integrated circuit packaging, copper interconnects, tin solder, copper nanocone array, graphene

Bonding technology is indispensable in electronic packaging, as it provides mechanical support and electrical interconnections between semiconductor chips. Reliability of bonding joints greatly influences the power consumption and performance of electronic systems, and thus it is essential to have a reliable bonding technology, especially when packaging density dramatically increases with device scaling. Copper (Cu) is the mainstream interconnect material, owing to its superior conductivity, in the existing complementary metal oxide semiconductor (CMOS) technology.[1] Lead−tin (Pb−Sn) eutectic was once a popular solder material in Cu bonding technology, the most widely used bonding technique, with a bonding temperature as low as 183 °C. Nevertheless, Pb is very hazardous and its usage in electronic products has been restricted by the European Union in 2003, spearheading the exploration of lead-free solders such as Sn−Ag−Cu and Sn−Cu eutectics.[2,3] To date, after more than a decade of research efforts, lead-free Cu bonding technology has been entangled in two critical issues limiting its reliability: high bonding temperature (∼260 °C) and aging degradation.[2,4,5] The prior issue increases not only the thermal budget of chip fabrication but also the failure rate for temperature-sensitive chips. The latter issue, induced by excessive growth of brittle intermetallic compounds (IMC) between the Sn solder and Cu substrate, significantly reduces the lifetime of bonding joints. To overcome these issues, a number of approaches have been attempted including ultrasonic bonding,[6] electrochemical deposition of metal nanostructures,[7−9] and metal sacrificial layer (Au or Ni).[10,11] Despite the effectiveness of these approaches in addressing either one of the issues, a solution that concurrently solves both issues remains elusive.

Here, we report a simple Sn−graphene−Cu-based bonding technology that is of low bonding temperature and high reliability. We electrochemically deposit a layer of Cu nanocone array on the Cu substrate and cover it with a graphene sheet,
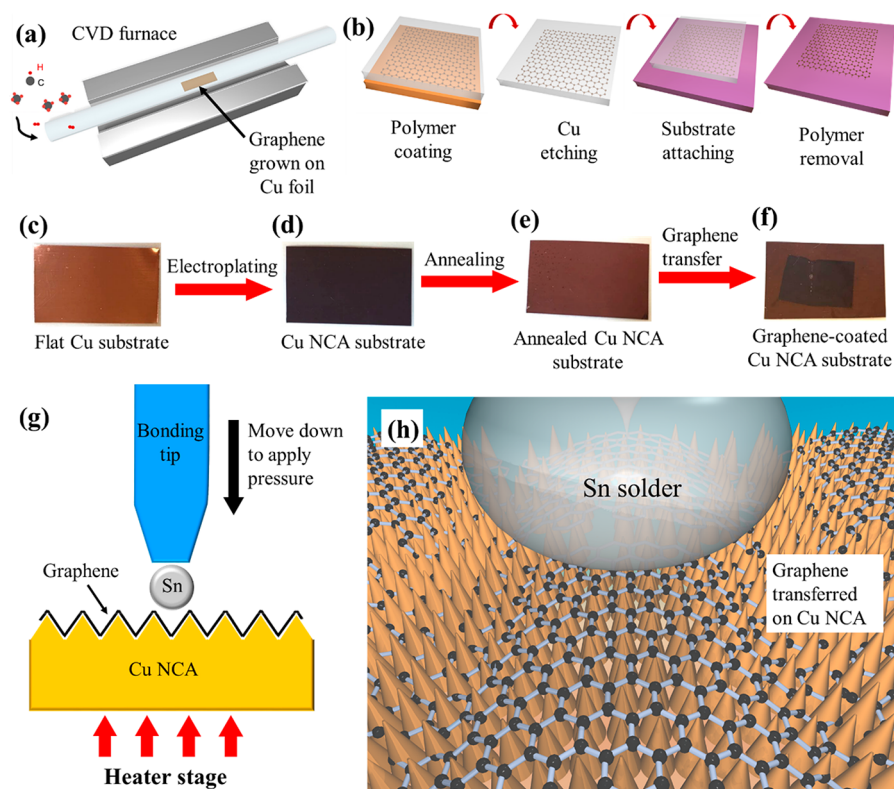
Figure 1. Schematics of the process showing the fabrication steps of our Sn−graphene−Cu bonds. (a) Large-area monolayer graphene is first synthesized on Cu foil *via* the LPCVD technique. (b) A layer of polymer is spin-coated on the synthesized graphene as a support layer followed by etching of the Cu foil. Subsequently, an annealed Cu nanocone array (Cu NCA) substrate is used to fish out the polymer-supported graphene film. The polymer is then removed in a solvent, resulting in a graphene-coated Cu NCA substrate. (c−f) Photographs of (c) a commercial C194 Cu substrate (2 cm × 1 cm), (d) an as-fabricated Cu NCA substrate, (e) an annealed Cu NCA substrate, and (f) a graphene-coated Cu NCA substrate. (g) A commercial bonding tester is then used to solder the Sn−Ag−Cu eutectic to the graphene-coated Cu NCA substrate. (h) Illustrated zoomed-in view of a good Sn−graphene−Cu bond. Schematics shown in (g) and (h) are only for illustration purposes, and the features are out of scale.

prior to thermocompression bonding. When subjected to heat, microscale Sn solder deforms and replicates the Cu nanocone array morphology, hence introducing nanoscale features in Sn. It is worth noting that the mechanical strengths of nanoscale Cu and Sn have opposite dependence on their sizes. "Smaller is stronger" for nanoscale Cu and "smaller is weaker" for nanoscale Sn, due to the much lower melting point of Sn and facile surface diffusion.[12−14] Since nanoscale Sn is weaker than its microscale form, lower energy is required for it to deform and uniformly distribute on the Cu substrate, forming Sn−Cu metallurgical bonds. In contrast, the Cu nanocone array does not deform at the same temperature due to its higher melting point and ultrahigh strength.[3] This phenomenon effectively contributes to a lower bonding temperature in our bonding technology. On the other hand, by inserting graphene, a one-atom-thick carbon sheet that is highly conductive and mechanically robust,[15,16] as an interlayer between Sn solder and Cu substrate to retard the growth of IMCs, effectively impedes the aging issue. Notably, a monolayer graphene sheet is capable of protecting the underlying Cu substrate from oxidation[17] and diffusion.[18] In addition, a graphene−Cu-layered composite has a superior mechanical strength,[19] thermal conductivity,[20] and resistance to fatigue damage[21] compared to Cu of the same dimension, as the graphene interlayer blocks dislocations in Cu. Through shear strength analyses, we demonstrate that, for the same aging duration, the shear strength of Sn−Cu joints degrades by 2-fold, while insertion of a graphene interlayer

successfully preserves the shear strength of Sn−Cu joints, with no observable degradation, confirming that our bonding technology is highly reliable. Importantly, our lead-free Cu bonding technology creates reliable bonding joints at 150 °C, which is lower than that in harmful lead-based Cu bonding technology (183 °C).

RESULTS AND DISCUSSION

In our low-temperature Cu bonding technology, the fabrication of a nanoscale graphene/Cu composite involves only three steps: deposition of the Cu nanocone array (NCA) and synthesis and transfer of graphene. Figure 1 illustrates how the fabrication processes of the nanoscale graphene/Cu composite can be integrated into the Cu bonding technology (see Methods for details). Large-area monolayer graphene was first synthesized on a Cu foil using low-pressure chemical vapor deposition (LPCVD) (Figure 1a). A layer of polymer was spin-coated on the synthesized graphene as a support layer followed by etching of the Cu foil (Figure 1b). In addition, Cu NCA was electroless plated on a commercial flat Cu substrate (Figure 1c,d). The as-fabricated Cu NCA substrate has a very rough surface and sharp tips with a tip diameter of ∼20 nm (Figure S1a). The bases of cones show an average diameter of ∼2 μm, while the cones' height is about 2−4 μm. The Cu NCA substrate was then annealed at 250 °C in a forming gas environment for 1 h (Figure 1e). Subsequently, the annealed Cu NCA substrate was used to scoop out the polymer-
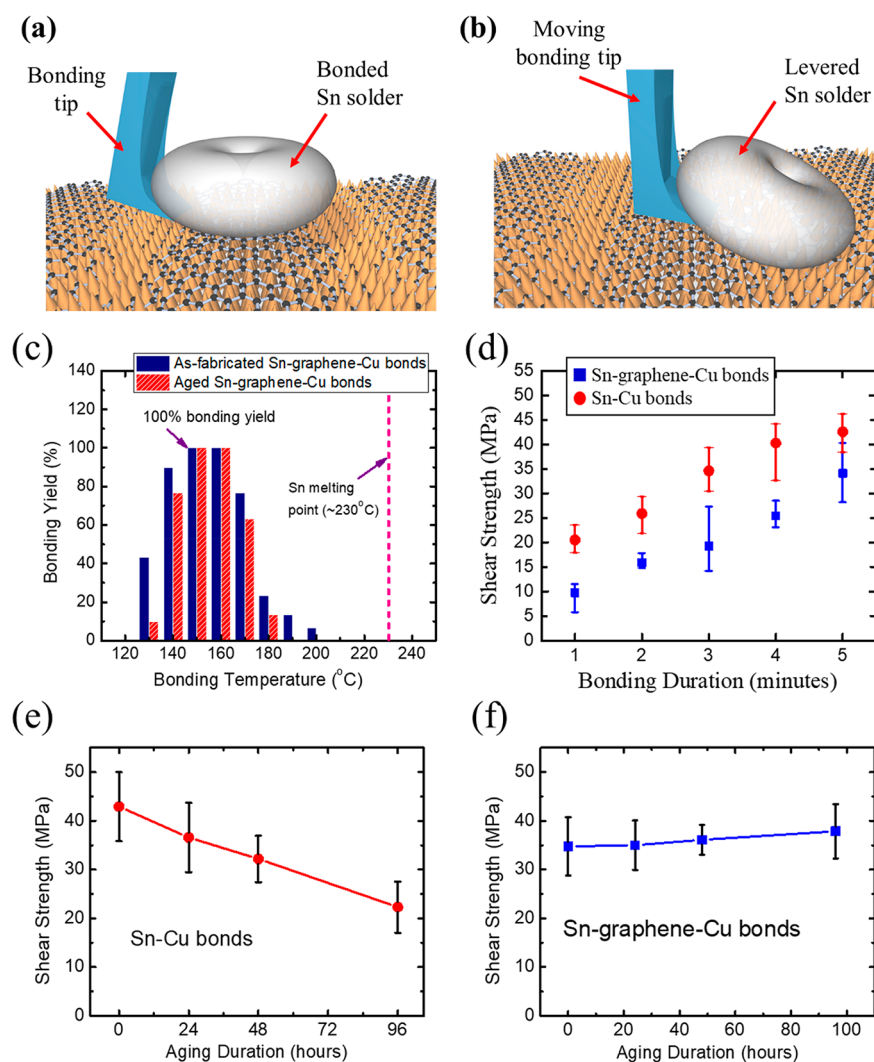
Figure 2. Shear strength test results of our Sn−graphene−Cu bonds. (a, b) Schematics showing how a shear strength test is performed. A bonding tip is first brought to the side of a bonded Sn solder (a) and then set to move horizontally with increasing force. The tip stops moving once the Sn solder was levered (b), and the bonding tester records the shear force required. Shear strength of a bond can be extracted by taking the maximum shear force required to lever the Sn solder and dividing by the measured area size of the bond. (c) Bonding yield of the Sn−graphene−Cu bond as a function of bonding temperature. Each group of data was collected from 30 bonds. (d) Shear strength distribution of both the Sn−Cu and Sn−graphene−Cu bonds as a function of bonding duration. Each average value was collected from five bonds. (e) Shear strength distribution of the Sn−Cu bonds as a function of aging duration. The average shear strength degrades with aging duration up to 2-fold for only 96 h of aging. (f) Shear strength distribution of the Sn−graphene−Cu bonds as a function of aging duration. Our Sn−graphene−Cu bonds are very robust and show no degradation in terms of average shear strength, after the same 96 h of aging.

supported graphene film. The sample was initially blow-dried with N_2, followed by 80 °C oven-baking. After that, the polymer support layer was removed in the solvent, leaving behind a graphene-coated Cu NCA substrate (Figure 1f). Finally, a commercial bonding tester was used to solder a Sn−Ag−Cu eutectic (760 μm diameter) to the graphene-coated Cu NCA substrate, by applying a constant force of 1500 gf (∼14.7 N) to the substrate for 5 min at 150 °C (Figure 1g). In this study, a Sn−Ag−Cu eutectic was chosen, as it is the most promising substitute for Sn−Pb solder among hundreds of lead-free candidates.[22−24] Figure 1h shows an illustration of a good Sn−graphene−Cu soldering joint. It is worth noting that direct synthesis of monolayer graphene on the Cu NCA substrate is currently challenging, as the nanocone structures would have collapsed at the present graphene growth temperatures (Figure S1b).

We have been able to observe a 100% bonding yield in our Sn−graphene−Cu joints fabricated at low bonding temperatures (150−160 °C) and that is maintained even after 96 h of aging. For this study, we define bonding yield as the ratio of solder joints with shear strength greater than 20 MPa to the number of solder joints tested. Specifically, from previous studies, 20 MPa has been considered as the minimum shear strength for an effective bonding between the Cu NCA and the Sn−Ag−Cu solder.[25] In this research, bonding yield remains 100% if we slightly increase the shear strength criterion to 25 MPa, as shown in Figure S2a. To extract the shear strength of each bond, we conducted a shear strength test using a Rhesca PTR-1101 commercial bonding tester. As illustrated in Figure 2a,b, a bonding tip was first brought to the side of a bonded Sn solder and then set to move horizontally with increasing force. The tip stops moving once the Sn solder was scraped off from the Cu NCA substrate, and the bonding tester records the
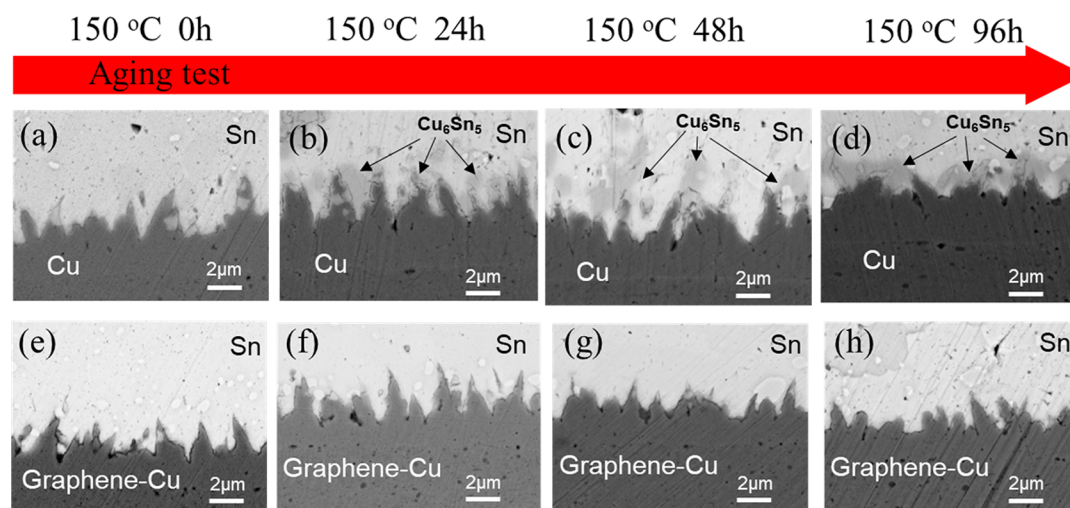
Figure 3. Aging behavior comparison between Sn−Cu and Sn−graphene−Cu bonds. An aging test is performed by baking each sample in an oven at 150 °C for different durations as indicated. (a−d) Cross-sectional SEM images of Sn−Cu bonds when they were as-fabricated and aged for different durations as indicated (*i.e.*, 24, 48, and 96 h). An intermetallic compound (IMC) such as Cu_6Sn_5 gradually grows with aging duration. (e−h) Cross-sectional SEM images of Sn−graphene−Cu bonds when they were as-fabricated and aged for different durations as indicated. Insertion of graphene interlayer effectively retards the growth of a Cu_6Sn_5 IMC, even after 96 h of aging.

required shear force. The shear strength of each solder joint was then calculated by taking the maximum shear force required to lever the Sn solder and dividing by the measured area size of the solder joint.

More than 210 Sn−graphene−Cu bonds were fabricated at seven different bonding temperatures (130, 140, 150, 160, 170, 200, and 230 °C). Each bonding yield was collected from at least 30 bonds. Figure 2c shows the bonding yield of our Sn−graphene−Cu bonds, when they were as-fabricated and aged, as a function of bonding temperature. For comparison, we have fabricated the same amount of bonds at each bonding temperature using the same approach, but without the graphene interlayer, namely, Sn−Cu bonds, and the bonding yield of Sn−Cu bonds is plotted in Figure S2b. As can be seen from Figures 2c and S2b, the bonding yield of both Sn−graphene−Cu and Sn−Cu bonds shows a consistent trend. Specifically, the bonding yield increases with temperature initially and achieves 100% when the bonding temperature rises to 150 °C. This observation is supported by an earlier study that proved that the creep rate of the Sn−Ag eutectic increases with temperature and shows an abrupt increase at 150 °C.[26] In addition, Tian *et al.* found that nanoscale Sn deforms based on diffusional plasticity such as Nabbarro-Herring or Coble creep.[14] As discussed earlier, a solid Sn solder requires a certain amount of energy to deform and uniformly distribute on the Cu substrate. At 150 °C, the sudden increase in Sn creep rate allows it to distribute at a faster rate on the Cu substrate, forming Sn−Cu metallurgical bonds. Consequently, the Sn−Cu bond fabricated at 150 °C is strong with relatively high yield. Apart from that, in the absence of Cu NCA, Sn−Cu bonds between the Sn solder and flat Cu substrate are normally fabricated at temperatures higher than 220 °C because the Sn solder is hard and does not deform well below 220 °C. We note that the Sn solder deforms at a lower temperature in our bonding technology as the melting point of Sn systematically reduces with decreasing size.[27] For example, the melting point of a Sn particle with 10 nm diameter is only ∼160 °C.[27] On the other hand, for bonding temperatures higher than 180 °C, the bonding yield of both Sn−graphene−Cu and Sn−Cu bonds

drastically drops with increasing temperatures (Figures 2c and S2b). This phenomenon can be attributed to the partial collapse of Cu NCA as the tensile strength in Cu becomes weaker and weaker when temperature increases.[28] All bonds were then subjected to a 96 h aging, and the bonding yield of aged bonds is also plotted in Figures 2c and S2b, for comparison purposes. Typically, the bonding yield of aged bonds is much lower compared to that of as-fabricated bonds. However, the bonding yield of aged Sn−graphene−Cu bonds fabricated at 150 and 160 °C remains at 100%, while that of all aged Sn−Cu bonds shows severe degradation, regardless of the bonding temperature. These results suggest that the insertion of a graphene interlayer at the Sn−Cu bonds plays a significant role in impeding the aging degradation issue.

We further note that the shear strength of each bond strongly relies on the bonding duration. In Figure 2d, we compare the as-fabricated shear strength of both Sn−graphene−Cu and Sn−Cu bonds made with different bonding duration, varying from 1 to 5 min. Each group of data was collected from five bonding joints. We observe that the as-fabricated shear strength of both types of bond increases with bonding duration. For 5 min of bonding duration, the average shear strength of Sn−Cu bonds (42 ± 4 MPa) is slightly larger than that of Sn−graphene−Cu (34 ± 6 MPa), when the bonds were freshly made. These results suggest the presence of graphene indeed hindered Sn and Cu from bonding with each other, but as the thickness of graphene is only one atomic layer, such effect is minor, and effective bonds can still form when the bonding duration is 4 min or longer. On the other hand, the average shear strength of Sn−Cu bonds degrades by 2-fold following 96 h of aging (Figure 2e). In contrast, our Sn−graphene−Cu bonds are very robust and show no observable degradation in terms of average shear strength, following the same 96 h of aging (Figure 2f). These observations show that, with the presence of a one-atom-thick graphene interlayer, the aging degradation is effectively avoided.

To understand how the insertion of a graphene interlayer at the Sn−Cu bonds helps in addressing the aging degradation issue, we performed a series of scanning electron microscopy
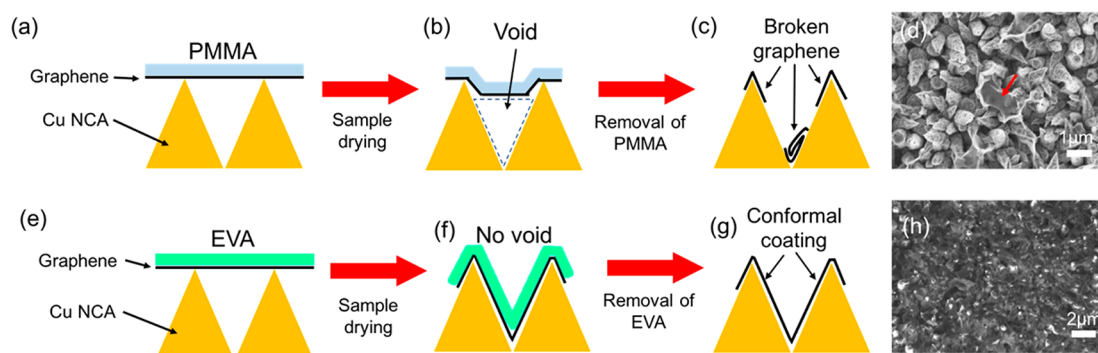
Figure 4. Comparison of PMMA- and EVA-assisted graphene transfer yield on a Cu NCA substrate. (a) Schematic of the situation when the PMMA/graphene stack is first brought into proximity of Cu NCA in deionized water. (b) A void is formed between the graphene and Cu NCA after sample drying due to the rigidity of PMMA. (c) Graphene tears apart once the PMMA support layer is removed. (d) Typical SEM image of the graphene transferred on Cu NCA using a PMMA support layer. The arrow indicates the broken graphene sheet dangling on the Cu NCA. (e) Schematic of the situation when the EVA/graphene stack is first brought into proximity of Cu NCA in deionized water. (f) No void is formed between the graphene and Cu NCA after the sample drying. (g) Graphene remains as a perfect sheet adhering to the Cu NCA substrate after the removal of the EVA support layer. (h) Typical SEM image of the graphene transferred on the Cu NCA substrate using an EVA support layer. The transferred graphene remains as a sheet and uniformly covers the Cu NCA substrate.
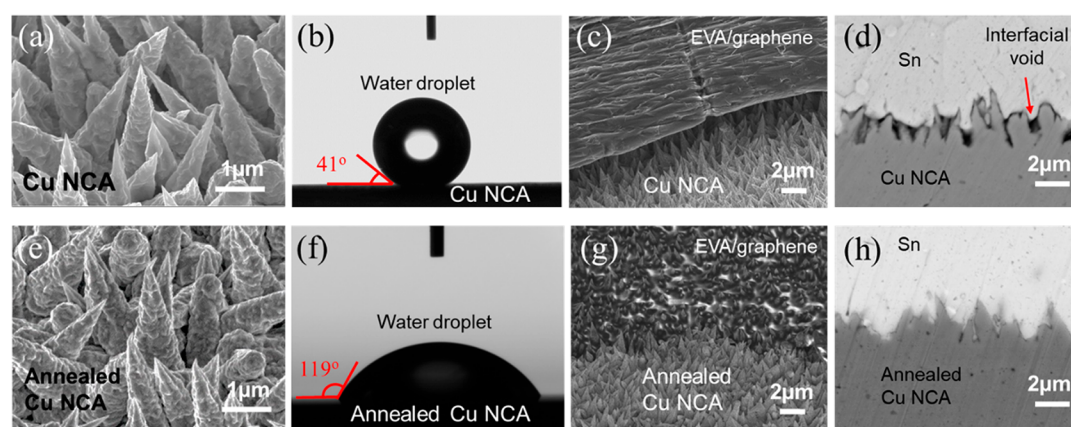

Figure 5. Impact of annealing treatment on the quality of the Sn−graphene−Cu bond. (a) Typical 45° tilted SEM image of an as-fabricated Cu NCA surface. (b) High-speed image of a water droplet on the Cu NCA surface, confirming that it is hydrophobic. (c) Typical 45° tilted SEM image showing how loosely the EVA-supported graphene stack lies on the hydrophobic Cu NCA surface. (d) Typical cross-sectional SEM image of an as-fabricated Sn−graphene−Cu bond fabricated using the hydrophobic Cu NCA substrate. Multiple interfacial voids formed at the Sn−graphene−Cu interface. (e) Typical 45° tilted SEM image of an annealed Cu NCA surface. (f) High-speed image of a water droplet on the annealed Cu NCA substrate indicating that it is hydrophilic. (g) Typical 45° tilted SEM image showing how good the EVA-supported graphene stack adheres to the annealed Cu NCA valleys. (h) Typical cross-sectional SEM image of an as-fabricated Sn−graphene−Cu bond fabricated using the hydrophilic Cu NCA substrate. No interfacial void is observed at the Sn−graphene−Cu interface.

(SEM) analyses on both Sn−Cu and Sn−graphene−Cu bonds when they were as-fabricated and aged for different duration (*i.e.*, 24, 48, and 96 h), as shown in Figure 3. We observe excessive growth of a scallop-like IMC along the Sn−Cu interface following the 24 h of aging (Figure 3b), and the IMC gradually grows into a μm-thick continuous layer following the 96 h of aging (Figure 3d). These observations are consistent with previous reports, and the IMC formed has been identified as Cu_6Sn_5 through X-ray diffraction analysis, which is very brittle and induces severe aging degradation at the Sn−Cu bonds.[2,3] In contrast, we do not observe significant growth of an IMC along the Sn−graphene−Cu interface, even for the 96 h aged sample (Figure 3e−h). These results indicate that the insertion of a graphene interlayer impedes the aging degradation at the Sn−Cu bonds by effectively retarding the growth of a Cu_6Sn_5 IMC.

As mentioned earlier, the surface of the Cu NCA substrate is very rough and contains numerous valleys, as shown in Figure

S1a. Achieving a conformal graphene coating on rough Cu NCA is not easy, and the conventional poly(methyl methacrylate) (PMMA)-assisted graphene transfer technique cannot serve the purpose, as illustrated in Figure 4a−c. In the PMMA-assisted graphene transfer technique, the PMMA/graphene stack is first brought into proximity of the Cu NCA substrate in deionized (DI) water (Figure 4a). The sample is then dried in an oven. Due to the mechanical rigidity of PMMA, the PMMA/graphene stack does not conform to the rough features of Cu NCA well, leaving behind voids, as illustrated in Figure 4b. Consequently, tearing of graphene is often observed on the Cu NCA substrate once the PMMA layer is removed, presumably due to the large surface tension or an aggressive nitrogen stream, during the sample drying processes (Figure 4c,d). To overcome this problem, we utilized an ethylene-vinyl acetate (EVA)-assisted graphene transfer technique.[29] Specifically, EVA has a 20 times larger elastic modulus and higher elongation capability compared to PMMA. In the

EVA-assisted graphene transfer technique, the EVA/graphene stack is first brought into proximity of the Cu NCA substrate in DI water (Figure 4e). As the EVA/graphene is much more elastic than the PMMA/graphene case, conformal coating on the Cu NCA can be obtained (Figure 4f), and after EVA removal, a much better graphene coverage can be achieved (Figure 4g,h). Details of both graphene transfer techniques are available in the Methods section.

It is worth noting that the Cu NCA surface is super-hydrophilic as-fabricated,[30] but is easily oxidized once exposed to air and becomes hydrophobic, as confirmed by the water contact angle measurement (Figure 5a,b). To ensure a conformal graphene coating on the rough Cu NCA, it is essential to have a hydrophilic Cu NCA substrate prior to using it to fish out the EVA/graphene stack in DI water; otherwise the EVA/graphene stack will loosely lie on the hydrophobic Cu NCA surface (Figure 5c). Such loose attachment of the EVA/graphene stack to the underlying Cu NCA substrate may induce the formation of interfacial voids that seriously deteriorate the bonding quality and should be avoided (Figure 5d). To make the Cu NCA surface hydrophilic again, we annealed the Cu NCA substrate at 250 °C in a forming gas environment for 1 h, prior to using it to fish out the EVA/graphene stack in DI water. Figure 5e shows a typical SEM image of an annealed Cu NCA surface. As can be seen, some sharp NCA tips collapse but the cone-like morphology remains, similar to that in Figure 5a. Importantly, the annealed Cu NCA surface is hydrophilic, with a water contact angle of 119° (Figure 5f). Figure 5g shows a typical SEM image demonstrating the EVA-supported graphene stack adheres well to the annealed Cu NCA surface, along the edge of the transferred EVA/graphene stack. SEM images of other similar samples are shown in Figure S3. As can be seen in Figure S3c,d, the EVA/graphene stack nicely conforms to the Cu NCA morphology in the sample's central region. This minimizes the formation of interfacial voids at the Sn−Cu interface, as confirmed by cross-sectional SEM analysis (Figure 5h). Overall, the results suggest that both EVA-assisted polymer transfer and a hydrophilic Cu NCA surface are critical to ensure conformal adhesion of graphene on the Cu NCA substrate, optimizing the bonding quality.

In our bonding technology, graphene at the Sn−Cu interface effectively retards the growth of the IMC layer, thus impeding the aging degradation. The results further indicate that the one-atom-thick monolayer graphene preserves the advantages of the nanocone array in lowering the bonding temperature. Despite its one-atom thickness, the large-area graphene used must be able to restrict Sn from diffusing into Cu, forming an IMC layer, and hence it must be of good quality. Through systematic material characterizations, we show that our CVD-grown large-area graphene is of monolayer thickness and good quality (Figure S4). For material characterizations, we transferred the CVD graphene grown on Cu foil to a Si/SiO₂ substrate with an oxide thickness of 285 nm, except for the transmission electronic microscopy (TEM) studies. The Raman spectrum taken from the graphene transferred on a Si/SiO₂ substrate is shown in Figure S4a. The full width at half-maximum (fwhm) of the 2D band for the as-transferred CVD graphene is ~36 cm⁻¹, and the D/G peak intensity ratio is 0.3, indicating that it is a single layer and has a low defect level. The Raman spectra taken from a bare Cu NCA substrate and graphene-coated Cu NCA substrate are included in Figure S4a for comparisons. As can be seen, the Raman spectrum taken from the graphene-coated Cu NCA substrate contains three characteristic peaks of graphene (*i.e.*, D, G, and 2D), similar to that of graphene transferred on the Si/SiO₂ substrate, indicating successful transfer of graphene on the Cu NCA substrate. We note that the characteristic peaks of graphene are weaker on the Cu NCA substrate, as the substrate has a strong Raman background signal (Figure S4a). Through SEM and atomic force microscopy (AFM) studies, we observe that the graphene transferred on the Si/SiO₂ substrate is a continuous film with the presence of some unavoidable wrinkles and polymer residue, indicating the quality of our EVA-assisted transfer technique (Figure S4b,c).[29] For TEM studies, we transferred the CVD-grown graphene to a Quantifoil electron microscopy holey grid (Figure S4d). As can be seen in Figure S4e, our CVD-grown graphene shows a crystalline hexagonal symmetry diffraction pattern, indicating that it is single-crystalline with a lattice spacing of 0.224 nm. Figure S4f shows an aberration-corrected scanning transmission electronic microscopy (STEM) image of our graphene sample. The one layer of carbon atoms arranged in a honeycomb lattice can be clearly seen. Nevertheless, we note that the graphene coverage on the Cu NCA is not perfect (Figure 5g). Closer examination reveals that a small amount of nanosized holes still formed in the graphene (Figure S3a). Although, in our bonding technology, there are nanosized holes in graphene at some of the Cu NCA tips, no continuous IMC layer is formed at the Sn/Cu bonding interface. This implies that intermetallic diffusion occurs only within a minuscule area (most likely at the nanosized cone tips), forming a nanoscale IMC (as illustrated in Figure S5a,b), which are insensitive to flaws and less brittle compared to the IMC layer.[31]

CONCLUSIONS

In summary, we have devised a graphene-based Cu bonding technology with high reliability. Instead of a flat Cu substrate, we demonstrated that the insertion of the graphene/Cu NCA composite on the flat Cu substrate concurrently addresses the high-bonding-temperature and aging degradation issues, which have long been limiting the reliability of the lead-free Cu bonding technology. Specifically, nanoscale metal reduces the thermal budget by lowering the energy required to establish Sn−Cu metallurgical bonds. Graphene, on the other hand, retards the IMC growth and thus impedes the aging degradation, as confirmed through shear strength and SEM analyses. Importantly, our bonding technology creates reliable soldering joints with bonding temperature as low as 150 °C, lower than that of hazardous lead-based technology (183 °C). With the advancement in graphene synthesis and transfer technology, we show that the Sn−graphene−Cu bonding technology presented in this work can be integrated into the existing commercial Cu bonding technology for industrial applications in the foreseeable near future.

METHODS

Fabrication of a Copper Nanocone Array Substrate. The Cu NCA was fabricated on a commercial C194 Cu substrate (2 cm × 1 cm, shown in Figure 1c) using a one-step electroless plating approach. Prior to the electroless plating, the C194 Cu substrate was dipped in a degreasing solution for 120 s, followed by acid cleaning (20% H₂SO₄) for 30 s and PdCl₂ activation for 30 s. Subsequently, the Cu nanocone array was electroless plated on the Cu substrate in an electrolyte composed of CuSO₄·5H₂O (0.03 mol/L), NiSO₄·6H₂O (0.0024 mol/L), NaH₂PO₂·H₂O (0.24 mol/L), Na₃C₆H₅O₇·2H₂O (0.05 mol/L),

pH regulator buffer H₃BO₃ (0.50 mol/L), and crystallization modifier (*i.e.*, polyethylene glycol (5 ppm)). The electrolyte solution was maintained at a temperature of 65 °C and pH values of 7.5−9.5, adjusted using NaOH solution. After 20 min of electroless plating, the sample was rinsed with DI water and blown dry with N₂. Figures 1d and S1a show the as-fabricated Cu NCA on a commercial C194 Cu substrate. We note that the Cu NCA surface is superhydrophilic as-fabricated, but easily oxidizes once exposed to air and becomes hydrophobic, as confirmed by the water contact angle measurement (Figure 5b). To make its surface hydrophilic again, we annealed the Cu NCA substrate at 250 °C in a forming gas environment (200 sccm of H₂ and 200 sccm of Ar at atmospheric pressure) for 1 h.

Graphene Synthesis. For large-area monolayer graphene synthesis, 25 μm thick Cu foil purchased from Alfa Aesar (#13382), with 99.8% purity, was used as the growth substrate. Prior to the growth, the Cu foil was treated using commercial Ni etchant (nickel etchant TFB, Transense).[32] Graphene was then synthesized on the treated Cu foil in a LPCVD system. The Cu foil was first annealed at 1030 °C for 30 min in a hydrogen environment (10 sccm of H₂ at 320 mTorr). Subsequently, 3.5 sccm of methane (CH₄) was introduced to the LPCVD system for graphene synthesis, and the system was maintained at 1030 °C for another 30 min in a hydrogen environment. Finally, the furnace lid was flung open to let the sample cool quickly to room temperature.

EVA-Supported Graphene Transfer. EVA solution (Aldrich, vinyl acetate 40 wt %, 10 wt % dissolved in xylene) was first spun, at 4000 rpm for 60 s, on the graphene synthesized on Cu foil. The sample was then baked in an oven at 80 °C for 60 min. Subsequently, the sample was floated on top of the Cu etchant (copper etchant TFB, Transense) for 20 min to remove the Cu foil. The sample (EVA/graphene stack) was then rinsed with deionized water several times. Next, the targeted substrate (annealed Cu NCA substrate) was used to scoop out the EVA/graphene stack, and the sample was initially dried with a N₂ stream, followed by oven baking at 80 °C for more than 8 h. Finally, the sample was soaked in xylene at 80 °C for 20−30 min to remove the EVA film, leaving behind a Cu NCA substrate with a conformal graphene coating on it (Figures 1f and S3).

PMMA-Supported Graphene Transfer. PMMA 950 A5 (Microchem Inc.) was first spun, at 2500 rpm for 60 s, on the graphene synthesized on Cu foil. The sample was then baked in an oven at 80 °C for 60 min. Subsequently, the sample was floated on top of the Cu etchant (copper etchant TFB, Transense) for 20 min to remove the Cu foil. The sample (PMMA/graphene stack) was then rinsed with deionized water several times. Next, the targeted substrate (Cu NCA or Si/SiO₂ substrate) was used to scoop out the PMMA/graphene stack, and the sample was initially dried with a N₂ stream, followed by oven baking at 80 °C for more than 8 h. Finally, the sample was soaked in acetone at room temperature for more than 1 h to remove the PMMA film.

Bonding, Aging, and Shear Strength Tests. A modified Rhesca PTR-1101 bonding tester was used to make all Cu bonding, and the solder ball used is Sn-3.0Ag-0.5Cu (in wt %) with 760 μm diameter by applying a constant force of 1500 gf (∼14.7 N), throughout this work. The bonding duration and temperature used for each bond is 5 min and 150 °C, respectively, unless otherwise specified. For the aging test, the bonded samples were baked in an oven at 150 °C for a duration of 96 h, unless otherwise specified. For the shear strength test, a bonding tip installed on the Rhesca PTR-1101 bonding tester was first brought to the side of a bonded Sn solder and then set to move horizontally with increasing force (Figure 2a,b). The tip stops moving once the Sn solder was levered from the Cu NCA substrate, and the bonding tester records the shear force required. Shear strength of each bond was then calculated by taking the maximum shear force required to lever the Sn solder divided by the measured area size of the bond.

Graphene Characterization. The Raman measurement was carried out using a Horiba-Jobin Yvon system with a 532 nm Ar+ laser line. The laser power used was around 1 mW on the sample, and a 100× objective was used to focus the beam. The size of the laser beam on the sample was around 1 μm. An AFM topography image was obtained using a Veeco Digital Instrument Nanoscope III. Field-emission scanning electronic microscopy was conducted using a FEI-Sirion 200. For TEM studies, the graphene synthesized on Cu foil was transferred to a Quantifoil 1.2/1.3 Au grid (300 mesh) and then characterized using a FEI Tecnai G2. Aberration-corrected STEM was carried out using a Nion UltraSTEM100.

ASSOCIATED CONTENT

Ⓢ Supporting Information

The Supporting Information is available free of charge on the ACS Publications website at DOI: 10.1021/acsnano.7b07739.

> SEM characterization of the Cu NCA surface prior to and following graphene synthesis, bonding yield for Sn−graphene−Cu and Sn−Cu bonds, SEM characterization of EVA/graphene stack transferred on an annealed Cu NCA substrate, characterization of our CVD-grown monolayer graphene, bonding mechanism in a graphene sheet with nanosized holes, and Figures S1−S5 (PDF)

AUTHOR INFORMATION

Corresponding Authors
*E-mail: jingkong@mit.edu.
*E-mail: huanmin@sjtu.edu.cn.

ORCID Ⓞ
Wei Sun Leong: 0000-0001-8131-2468
Ju Li: 0000-0002-7841-8058
Jing Kong: 0000-0003-0551-1208

Author Contributions
#H. Wang, W. S. Leong, F. Hu, L. Ju, and C. Su contributed equally to this work.

Notes
The authors declare no competing financial interest.

ACKNOWLEDGMENTS

REFERENCES

(1) Lu, L.; Shen, Y.; Chen, X.; Qian, L.; Lu, K. Ultrahigh Strength and High Electrical Conductivity in Copper. *Science* **2004**, *304*, 422−426.

(2) Zeng, K.; Tu, K. N. Six Cases of Reliability Study of Pb-free Solder Joints in Electronic Packaging Technology. *Mater. Sci. Eng., R* **2002**, *38*, 55−105.

(3) Abtew, M.; Selvaduray, G. Lead-free Solders in Microelectronics. *Mater. Sci. Eng., R* **2000**, *27*, 95−141.

(4) Wang, J.; Wang, Q.; Wu, Z.; Tan, L.; Cai, J.; Wang, D. Plasma Combined Self-assembled Monolayer Pretreatment on Electroplated-Cu Surface for Low Temperature Cu−Sn Bonding in 3D Integration. *Appl. Surf. Sci.* **2017**, *403*, 525−530.

(5) Annuar, S.; Mahmoodian, R.; Hamdi, M.; Tu, K.-N. Intermetallic Compounds in 3D Integrated Circuits Technology: A Brief Review. *Sci. Technol. Adv. Mater.* **2017**, *18*, 693−703.

(6) Li, M.; Li, Z.; Xiao, Y.; Wang, C. Rapid Formation of Cu/Cu3Sn/Cu Joints Using Ultrasonic Bonding Process at Ambient Temperature. *Appl. Phys. Lett.* **2013**, *102*, 094104.

(7) Hsiao, H.-Y.; Liu, C.-M.; Lin, H.-w.; Liu, T.-C.; Lu, C.-L.; Huang, Y.-S.; Chen, C.; Tu, K. N. Unidirectional Growth of Microbumps on (111)-Oriented and Nanotwinned Copper. *Science* **2012**, *336*, 1007−1010.

(8) Luan, Q.; Bley, V.; Lebey, T.; Schlegel, B.; Menager, L. Nano Copper Wires Interconnection for Three—Dimensional Integration in Power Electronics. *Power Electron. Spec. Conf. (PESC)* **2008**, 278−281.

(9) Li, J.; Yu, X.; Shi, T.; Cheng, C.; Fan, J.; Cheng, S.; Liao, G.; Tang, Z. Low-Temperature and Low-Pressure Cu−Cu Bonding by Highly Sinterable Cu Nanoparticle Paste. *Nanoscale Res. Lett.* **2017**, *12*, 255.

(10) Guan, Y.; Ma, S.; Zeng, Q.; Meng, W.; Chen, J.; Jin, Y. Effect of Metallic Materials Films on the Properties of Copper/Tin Micro-Bump Thermo-Compression Bonding. *IEEE Electron. Compon. Technol. Conf.* **2017**, 1291−1296.

(11) Yu, Y.; Yan, C.; Zheng, Z. Polymer-Assisted Metal Deposition (PAMD): A Full-Solution Strategy for Flexible, Stretchable, Compressible, and Wearable Metal Conductors. *Adv. Mater.* **2014**, *26*, 5508−5516.

(12) Li, X.; Wei, Y.; Lu, L.; Lu, K.; Gao, H. Dislocation Nucleation Governed Softening and Maximum Strength in Nano-Twinned Metals. *Nature* **2010**, *464*, 877−880.

(13) Jang, D.; Li, X.; Gao, H.; Greer, J. R. Deformation Mechanisms in Nanotwinned Metal Nanopillars. *Nat. Nanotechnol.* **2012**, *7*, 594−601.

(14) Tian, L.; Li, J.; Sun, J.; Ma, E.; Shan, Z.-W. Visualizing Size-Dependent Deformation Mechanism Transition in Sn. *Sci. Rep.* **2013**, *3*, 2113.

(15) Novoselov, K. S.; Geim, A. K.; Morozov, S. V.; Jiang, D.; Zhang, Y.; Dubonos, S. V.; Grigorieva, I. V.; Firsov, A. A. Electric Field Effect in Atomically Thin Carbon Films. *Science* **2004**, *306*, 666−669.

(16) Lee, C.; Wei, X.; Kysar, J. W.; Hone, J. Measurement of the Elastic Properties and Intrinsic Strength of Monolayer Graphene. *Science* **2008**, *321*, 385−388.

(17) Chen, S.; Brown, L.; Levendorf, M.; Cai, W.; Ju, S.-Y.; Edgeworth, J.; Li, X.; Magnuson, C. W.; Velamakanni, A.; Piner, R. D.; Kang, J.; Park, J.; Ruoff, R. S. Oxidation Resistance of Graphene-Coated Cu and Cu/Ni Alloy. *ACS Nano* **2011**, *5*, 1321−1327.

(18) Li, L.; Chen, X.; Wang, C.-H.; Cao, J.; Lee, S.; Tang, A.; Ahn, C.; Singha Roy, S.; Arnold, M. S.; Wong, H.-S. P. Vertical and Lateral Copper Transport through Graphene Layers. *ACS Nano* **2015**, *9*, 8361−8367.

(19) Kim, Y.; Lee, J.; Yeom, M. S.; Shin, J. W.; Kim, H.; Cui, Y.; Kysar, J. W.; Hone, J.; Jung, Y.; Jeon, S.; Han, S. M. Strengthening Effect of Single-Atomic-Layer Graphene in Metal−Graphene Nano-layered Composites. *Nat. Commun.* **2013**, *4*, 2114.

(20) Goli, P.; Ning, H.; Li, X.; Lu, C. Y.; Novoselov, K. S.; Balandin, A. A. Thermal Properties of Graphene−Copper−Graphene Hetero-geneous Films. *Nano Lett.* **2014**, *14*, 1497−1503.

(21) Hwang, B.; Kim, W.; Kim, J.; Lee, S.; Lim, S.; Kim, S.; Oh, S. H.; Ryu, S.; Han, S. M. Role of Graphene in Reducing Fatigue Damage in Cu/Gr Nanolayered Composite. *Nano Lett.* **2017**, *17*, 4740−4745.

(22) He, S.; Nishikawa, H. Effect of Substrate Metallization on the Impact Strength of Sn-Ag-Cu Solder Bumps Fabricated in A Formic Acid Atmosphere. *Int. Conf. on Electron. Packag. (ICEP)* **2017**, 381−385.

(23) Wang, C.-h.; Chen, S.-w. Sn−0.7wt.%Cu/Ni Interfacial Reactions at 250°C. *Acta Mater.* **2006**, *54*, 247−253.

(24) Yoon, J.-W.; Kim, S.-W.; Jung, S.-B. IMC Morphology, Interfacial Reaction and Joint Reliability of Pb-Free Sn−Ag−Cu Solder on Electrolytic Ni BGA Substrate. *J. Alloys Compd.* **2005**, *392*, 247−252.

(25) Lu, Q.; Chen, Z.; Zhang, W.; Hu, A.; Li, M. Low-Temperature Solid State Bonding Method Based on Surface Cu−Ni Alloying Microcones. *Appl. Surf. Sci.* **2013**, *268*, 368−372.

(26) Mathew, M. D.; Yang, H.; Movva, S.; Murty, K. L. Creep Deformation Characteristics of Tin and Tin-Based Electronic Solder Alloys. *Metall. Mater. Trans. A* **2005**, *36*, 99−105.

(27) Lai, S. L.; Guo, J. Y.; Petrova, V.; Ramanath, G.; Allen, L. H. Size-Dependent Melting Properties of Small Tin Particles: Nano-calorimetric Measurements. *Phys. Rev. Lett.* **1996**, *77*, 99−102.

(28) Carreker, R. P.; Hibbard, W. R. Tensile Deformation of High-Purity Copper as A Function of Temperature, Strain Rate, and Grain Size. *Acta Metall.* **1953**, *1*, 654−663.

(29) Hong, J. Y.; Shin, Y. C.; Zubair, A.; Mao, Y.; Palacios, T.; Dresselhaus, M. S.; Kim, S. H.; Kong, J. A Rational Strategy for Graphene Transfer on Substrates with Rough Features. *Adv. Mater.* **2016**, *28*, 2382−2392.

(30) Deng, Y.; Ling, H.; Feng, X.; Hang, T.; Li, M. Electrodeposition and Characterization of Copper Nanocone Structures. *CrystEngComm* **2015**, *17*, 868−876.

(31) Gao, H.; Ji, B.; Jäger, I. L.; Arzt, E.; Fratzl, P. Materials Become Insensitive to Flaws at Nanoscale: Lessons from Nature. *Proc. Natl. Acad. Sci. U. S. A.* **2003**, *100*, 5597−5600.

(32) Kim, S. M.; Hsu, A.; Lee, Y.-H.; Dresselhaus, M. S.; Palacios, T.; Kim, K. K.; Kong, J. The Effect of Copper Pre-Cleaning on Graphene Synthesis. *Nanotechnology* **2013**, *24*, 365602.

Supporting Information

Low-Temperature Copper Bonding Strategy with

Graphene Interlayer

Haozhe Wang,[†,#] Wei Sun Leong,[†,#] Fengtian Hu,[‡,#] Longlong Ju,[‡,#] Cong Su,[§,#] Yukun Guo,[‡] Ju Li,[§]

Ming Li,[‡] Anmin Hu,[‡,] and Jing Kong[†,*]*

[†]Department of Electrical Engineering and Computer Science, Massachusetts Institute of Technology,

Cambridge, Massachusetts 02139, United States

[‡]School of Materials Science and Engineering, Shanghai Jiao Tong University, Shanghai, 200240,

China

[§]Department of Nuclear Science and Engineering, Massachusetts Institute of Technology, Cambridge,

Massachusetts, 02139, United States

[#]These authors contributed equally to this work.

*E-mail: jingkong@mit.edu.

*E-mail: huanmin@sjtu.edu.cn.

S1. SEM characterization of Cu NCA surface prior to and following the graphene synthesis
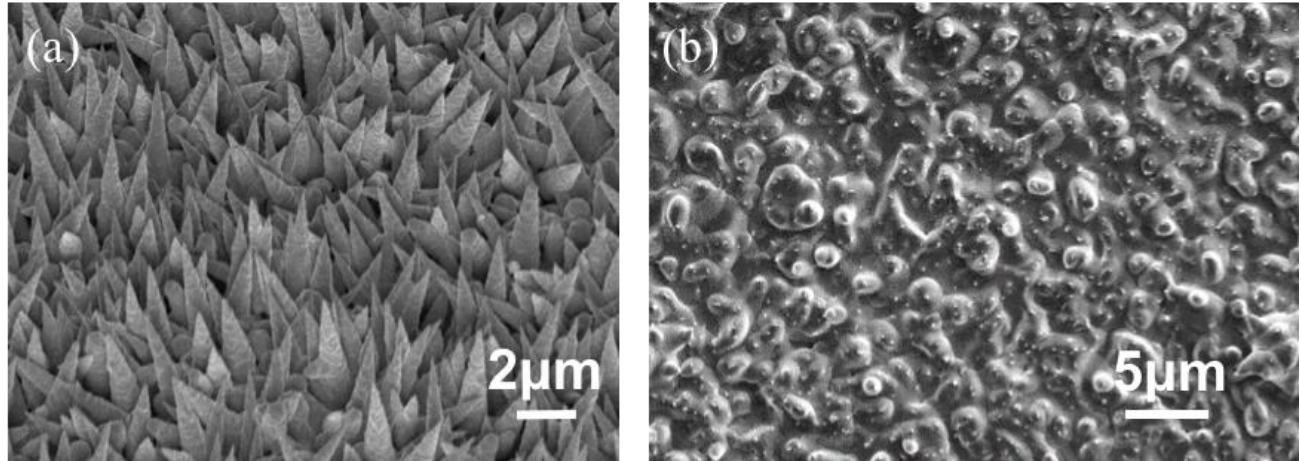

Figure S1. SEM characterization of Cu NCA surface prior to and following the graphene synthesis. (a) Typical SEM image of an as-fabricated Cu NCA surface. (b) Typical SEM image of the Cu NCA surface following the conventional LPCVD graphene growth process.

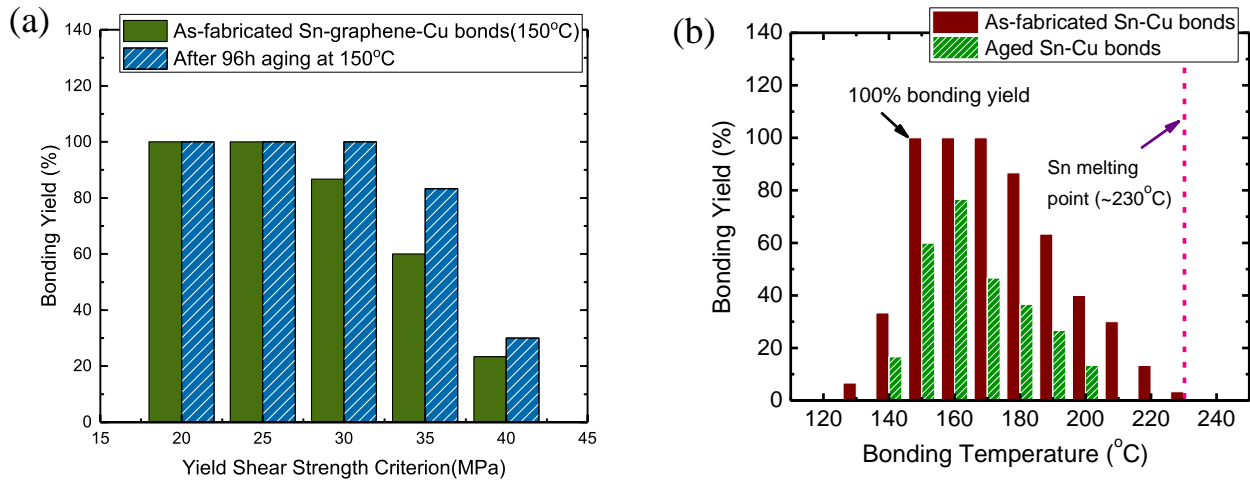## S2. Bonding yield for Sn-graphene-Cu and Sn-Cu bonds

Figure S2. (a) Bonding yield of the Sn-graphene-Cu bonds as a function of shear strength criterion when they were as-fabricated and aged. (b) For 20MPa shear strength, the bonding yield of the Sn-Cu bonds as a function of bonding temperature when they were as-fabricated and aged. Each group of data was collected from 30 bonds.
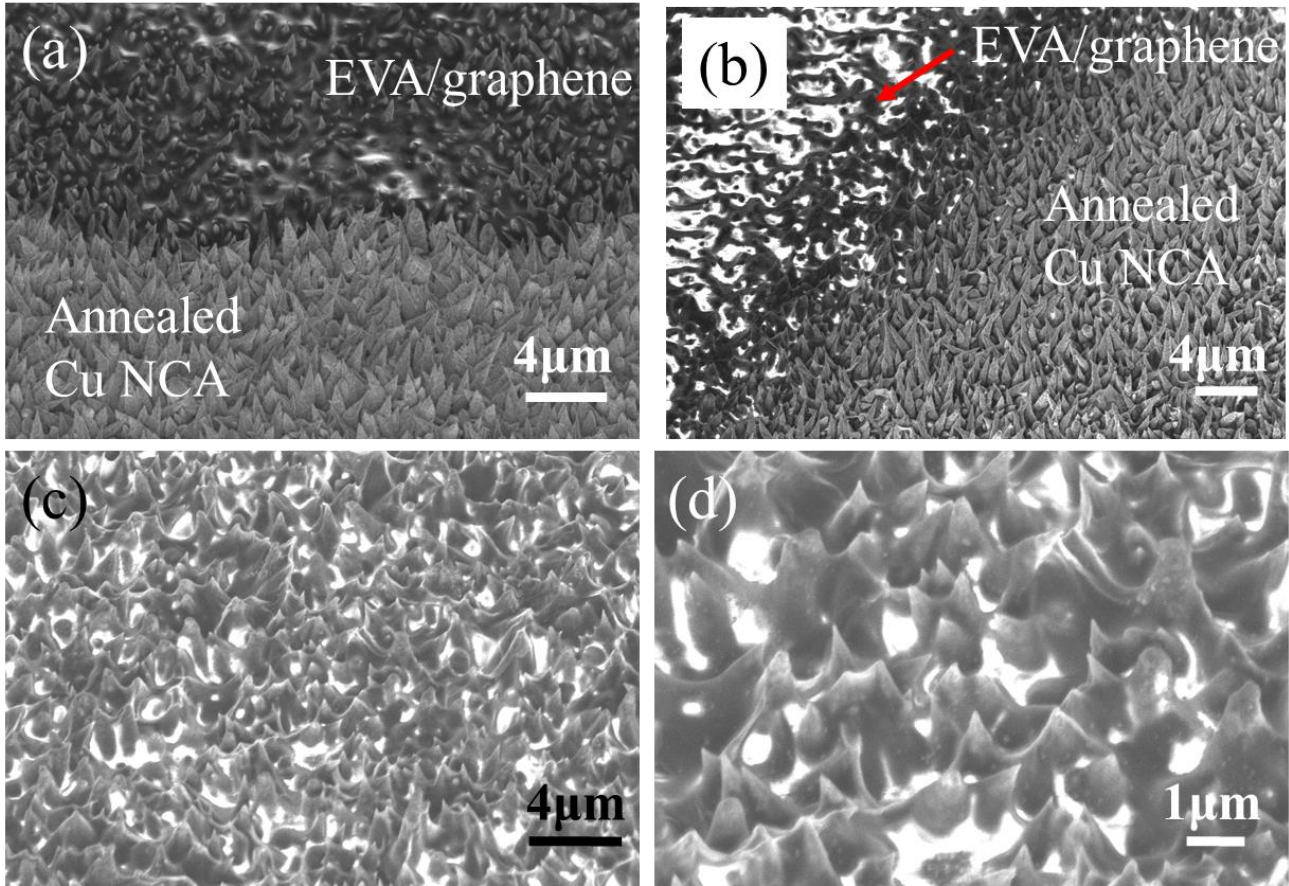
Figure S3. SEM characterization of a 15mm x 8 mm large EVA/graphene stack transferred to an annealed Cu NCA substrate (20mm x 10mm). (a-b) Typical 45° tilted SEM images showing how good the EVA/graphene stack adheres to the annealed Cu NCA surface, along the edge of transferred EVA/graphene stack. (c) Typical 45° tilted SEM images showing central region of the EVA/graphene stack as-transferred on the annealed Cu NCA substrate. (d) Higher magnification SEM image of the sample's central region showing how good the EVA/graphene stack conforms to the nanocone valley in the Cu NCA substrate.

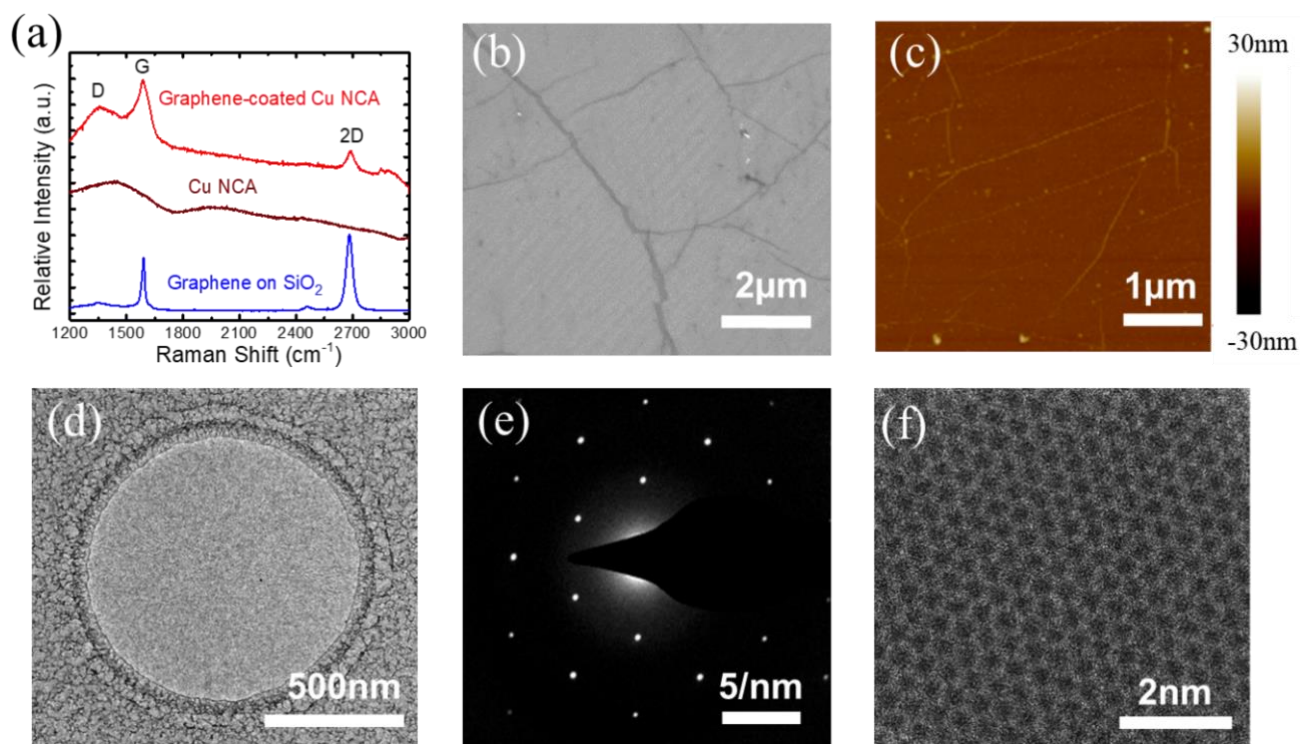## S4. Characterization of our CVD-grown monolayer graphene

Figure S4. Characterization of our CVD-grown monolayer graphene. (a) Typical Raman spectrum taken from graphene transferred on a Si/SiO$_2$ substrate, bare Cu NCA substrate, and graphene transferred on Cu NCA substrate, respectively. (b) Typical SEM image of a monolayer graphene transferred on Si/SiO$_2$ substrate. (c) Typical AFM image of a monolayer graphene transferred on a Si/SiO$_2$ substrate. (d) Typical TEM image of a monolayer graphene transferred on a Quantifoil® electron microscopy holey grid. (e) Diffraction pattern of the graphene sample shown in d. (f) Aberration-corrected STEM image of the graphene sample.

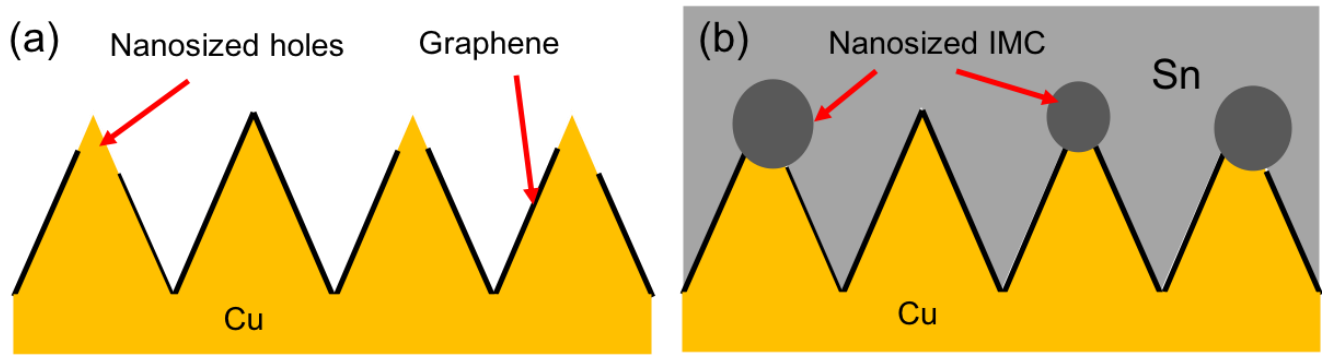## S5. Bonding mechanism in a graphene sheet with nanosized holes

Figure S5. Schematic illustration of bonding mechanism in a graphene sheet with nanosized holes. (a)

Graphene sheet with nanosized holes. (b) Nanosized Cu-Sn intermetallic compounds (IMC) formed.